Integrated Coupled Inductors with Functionality of Current Balancing Transformer for Two-Phase Synchronous DC-DC Converters

Dou, Yi; Ouyang, Ziwei; Andersen, Michael A. E.

Published in:
IEEE Transactions on Power Electronics

Link to article, DOI:
10.1109/TPEL.2019.2948882

Publication date:
2020

Document Version
Peer reviewed version

Integrated Coupled Inductors with Functionality of Current Balancing Transformer for Two-Phase Synchronous DC-DC Converters

Yi Dou, *Student Member, IEEE,* Ziwei Ouyang, *Senior Member, IEEE,* and Michael A.E. Andersen, *Member, IEEE,*

***Abstract*—With the emerging technology of wide-band-gap power semiconductors and modern ferrite materials, the switching frequency of DC-DC converters can be pushed to mega-hertz range to achieve higher power density. In order to deal with a high conduction current, multi-phase converters are adopted to distribute the current for both power devices and windings. However, the current unbalance among phases may cause unexpected power loss to the converters. In this letter, the current unbalance issue is addressed by an integrated current balancing transformer for a two-phase DC-DC converter. The current of two phases in the converter can be automatically compensated to be identical by the proposed structure, which also reduces the complexity of the control system. A 1 MHz GaN based two-phase buck converter is built to verify the proposed structure and its efficiency achieves 97.5% at 4 V/6 A output with the ZVS turn-on of the switches.**

***Index Terms*—high-frequency DC-DC converter, magnetic integration, GaN HEMTs, current balancing transformer**

I. Introduction

With the rapid development of wide-band-gap (WBD) semiconductors, especially GaN HEMTs, the switching frequency of DC-DC converters can be pushed to mega-hertz (MHz) range to reduce the size of magnetic devices and to achieve higher power density. At the high frequency operation of the GaN HEMTs, the achievement of ZVS turn-on is of great importance to minimize the switching loss and to address the critical EMI issues [1]. Thus, the Critical Conduction Mode (CRM) operation is widely used to achieve ZVS turn-on in high-frequency converters, such as bi-directional DC-DC converters [2] and PFC converters [3]. However, a main drawback in CRM converters is that the current ripple may cause high conduction loss both on semiconductors and on windings of the magnetic devices [4]. Consequently, multi-phase converters are proposed by distributing the current into several phases to reduce the conduction loss but it sacrifices the number of components, the complexity of control and the converters' cost [5].

The coupled inductor (CI) has been introduced into multi-phase ZVS converters, including buck converters [6] and boost PFC converters [7]. With the coupled inductor and the interleaved operation, the ZVS turn-on can be realized for all the switches and the current ripple can also be reduced. However, the interleaved operation needs a very precise control of driving signals to maintain the ZVS turn-on for the switches, which is even more difficult for multi-phase operation due to high requirement for the controller, especially at mega-hertz switching frequency. In addition, in the multi-phase converters with coupled inductors, the current unbalance issue may cause extra power loss on magnetic devices and create uneven hot-spots on the converters, which puts forward higher requirement for the thermal management for the system. Conventionally, this issue can be addressed by the regulation with complex control strategy and extra current/ voltage sensors [8]. However, this solution is not acceptable in low-power applications. In this letter, a new magnetic structure is proposed to address the problem by balancing the current in a two-phase converter and maintaining the ZVS turn-on capability, as shown in Fig. 1 [9]. A 1 MHz proof-of-concept prototype is built, whose equivalent circuit is shown in Fig. 2, to verify the proposed structure. The two phases of the buck converter works at the synchronous mode, thus only one PWM signal is required to

Yi Dou, Ziwei Ouyang and Michael A.E. Andersen are with Department of Electrical Engineering, Technical University of Denmark, Kgs. Lyngby, Denmark. (E-mail: yidou,zo,ma@elektro.dtu.dk)

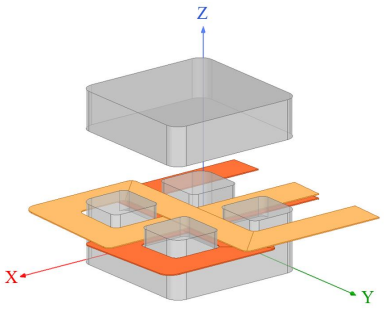

Fig. 1. Illustration of the proposed magnetic structure.

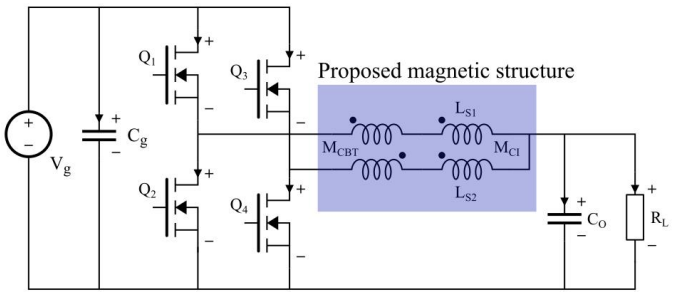

Fig. 2. Topology of the prototype: two-phase Buck converter with direct coupled inductor and integrated current balancing transformer.

drive the switches and the identical dead-time can be utilized under the balanced current for both of the phases, which further simplifies the control system. The rest of the letter is arranged as: Section II introduces the operation principle of the current balancing transformer and the structure of the proposed integrated magnetic device; Section III introduces the magnetic reluctance model for the proposed structure; The experimental verification is presented in section IV and finally the section V concludes the letter.

II. Direct Coupled Inductor with Integrated Current Balancing Transformer

A. Principle of current balancing transformer (CBT)

The current balancing transformer is introduced into multi-phase DC-DC converters to deal with current unbalance caused by mismatched inductance and driving signals [10]. The operational principle of CBT is presented firstly to provide the foundation of the proposed magnetic structure. In Fig. 3, the structure of a CBT with a U-type core, whose effective area is A_e and the equivalent length of magnetic flux is L_c, is illustrated and the current of phase 1 and phase 2 (i_{P1} and i_{P2}) is added as the excitation of the CBT. The CBT windings in phase 1 are reversely coupled with the windings in phase 2 to achieve the automatically balancing function. Due to the mismatching of the inductance and driving signals, the current changing rate in phase 1 and phase 2 ($\frac{\mathrm{d}i_{P1}}{\mathrm{d}t}$ and $\frac{\mathrm{d}i_{P2}}{\mathrm{d}t}$) are different. Assuming the current changing rate in phase 1 is higher than that in phase 2, the relation can be given by

$$\frac{\mathrm{d}i_{P1}}{\mathrm{d}t} > \frac{\mathrm{d}i_{P2}}{\mathrm{d}t} \tag{1}$$

Then the induced electromotive forces ($E.M.F.$) in phase 1 and phase 2 will be generated as the direction marked in Fig. 3 and described as

$$E.M.F = \mu A_e N^2 L_c \left(\frac{\mathrm{d}i_{P1}}{\mathrm{d}t} - \frac{\mathrm{d}i_{P2}}{\mathrm{d}t}\right) > 0 \tag{2}$$

, where μ is the effective permeability of the flux path and N is the number of turns for the CBT windings. Consequently, the induced current (i_{ind1} and i_{ind2}) will be generated to reduce the current in phase 1 and increase the current in phase 2 until the current changing rate in phase 1 and phase 2 are identical. It is noticed that the CBT can only balance the AC components of the current between two phases. Combining with the of natural feature of the power devices, which have a positive temperature coefficient, the conducted current of two phases can be maintained identical during the steady-state operation.

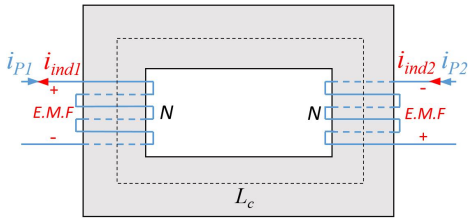

Fig. 3. Illustration of the operation principle for CBT.

B. Proposed integrated magnetic structure

Applying the concept of using CBT to solve the current unbalance issue, an integrated magnetic structure is proposed with a four-leg magnetic core to integrate a CBT with a coupled inductor, as illustrated in Fig. 1. The detailed winding configuration for the proposed structure is presented in Fig. 4: A one-turn winding for phase 1 is illustrated in the left and an one-turn winding in phase 2 is illustrated in the right; Each winding consists of 3 parts: the CI part marked in red, the CBT part marked in blue and the connection part, whose function is to build a multi-turn configuration, marked in green.

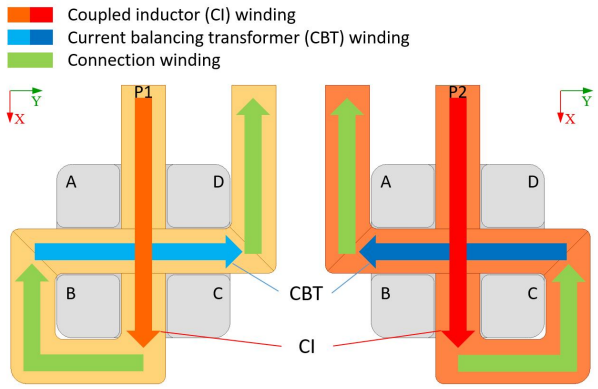

Fig. 4. Winding configuration for the proposed magnetic device.

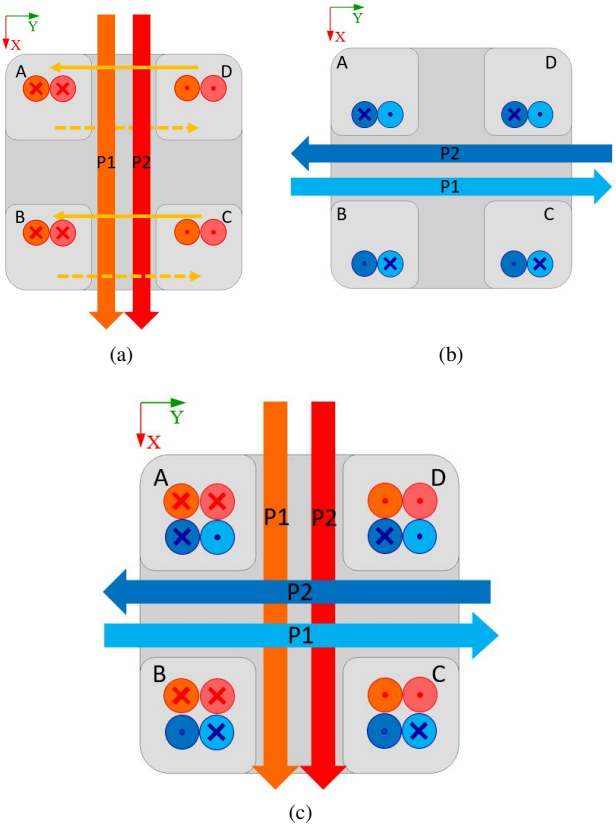

Fig. 5. Flux distribution of the proposed structure (a) For the CI winding (b) For the CBT winding (c) Overall distribution.

Since the CI winding and CBT winding are arranged as orthogonality, they are magnetically decoupled and their effective inductance can be modeled independently [10]. In Fig. 5(a), the magnetic flux of the CI windings is illustrated from the top view: The magnetic flux generated in section A and B points into the paper while the flux in section C and D points out of the paper. Thus, the flux generated by phase 1 and 2 are enhanced by each other, where a directly coupled inductor is formed. In Fig. 5(b), the magnetic flux of the CBT windings is illustrated and it can be found that the direction of flux generated by phase P2 is opposite to the flux generated by the phase P1. Thus, a CBT is formed and provides the current balancing function for the two phases as presented before. Finally, an overall flux distribution is illustrated in Fig. 5(c) with removing the connection part of the windings. With the CI windings and the CBT windings connected in series by the connection part, the CI and the CBT are connected in series in the equivalent circuit model, as shown in Fig. 2. Due to the inductance generated by the connection part is dominated by the permeability of air, thus their inductance can be neglected in the equivalent circuit model.

III. Reluctance Model of the Proposed Structure

In this section the magnetic reluctance model is built for the proposed structure to correlate its physical structure with its circuit model. Normally, the air-gap needs to be added into the path of the magnetic flux in an inductor to avoid the saturation of magnetic materials. In this structure, as the winding position illustrated in Fig. 5, the air-gaps can be put at all of the legs or can be settled only at leg A&B, or leg C&D while other configurations of the air-gaps will break the function of the CI or the CBT. Based on the analysis in the section II, the CI winding and the CBT winding are magnetically decoupled, thus two independent reluctance models can be built for the CT and the CBT, as illustrated in Fig. 6 and the value of each reluctance is given in Table I.

Based on the reluctance model, the self-inductance (L_{s1}, L_{s2}) and the mutual inductance (M) of the CI can be calculated as:

$$\begin{cases} L_{S1} = \dfrac{N_1^2}{\mathcal{R}_{TW} + \mathcal{R}_{BW} + \mathcal{R}_{AB} + \mathcal{R}_{CD}} \\ L_{S2} = \dfrac{N_2^2}{\mathcal{R}_{TW} + \mathcal{R}_{BW} + \mathcal{R}_{AB} + \mathcal{R}_{CD}} \\ M = \dfrac{N_1 N_2}{\mathcal{R}_{TW} + \mathcal{R}_{BW} + \mathcal{R}_{AB} + \mathcal{R}_{CD}} \end{cases} \tag{3}$$

,where N_1 and N_2 is the number of turns of the phase 1 and phase 2 for the CI winding, and the $\mathcal{R}_{AB}$ and the $\mathcal{R}_{CD}$ can be calculated by

$$\begin{cases} \mathcal{R}_{AB} = \dfrac{(\mathcal{R}_{AA} + \mathcal{R}_{LA})(\mathcal{R}_{AB} + \mathcal{R}_{LB})}{\mathcal{R}_{AA} + \mathcal{R}_{LA} + \mathcal{R}_{AB} + \mathcal{R}_{LB}} \\ \mathcal{R}_{CD} = \dfrac{(\mathcal{R}_{AC} + \mathcal{R}_{LC})(\mathcal{R}_{AD} + \mathcal{R}_{LD})}{\mathcal{R}_{AC} + \mathcal{R}_{LC} + \mathcal{R}_{AD} + \mathcal{R}_{LD}} \end{cases} \tag{4}$$

In the CBT, the number of turns for each phase must be designed as identical to achieve the current balance function and correspondingly the magnetizing inductance (M_{CBT}) can be calculated by:

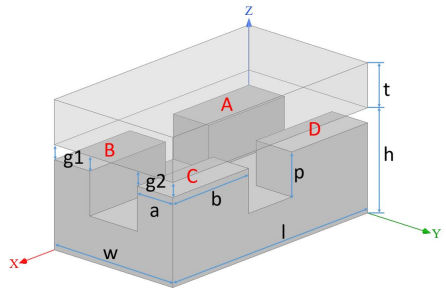

(a)

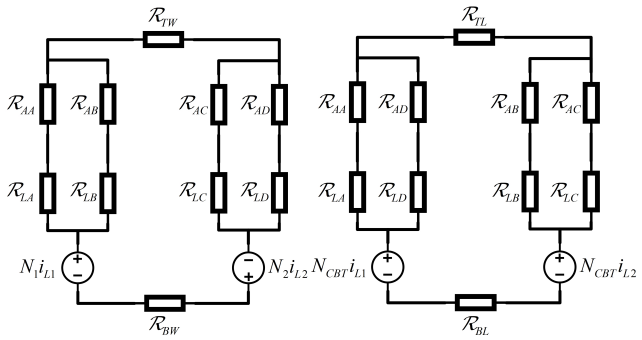

(b) (c)

Fig. 6. Decoupled reluctance model for the proposed structure (a) Physical size annotation (the corners of the core are simplified as orthogonal) (b) Reluctance model for the CI (c) Reluctance model for the CBT.

$$M_{CBT} = \frac{N_{CBT}^2}{\mathcal{R}_{TL} + \mathcal{R}_{BL} + \mathcal{R}_{AD} + \mathcal{R}_{BC}} \tag{5}$$

, where N_{CBT} is the number of turns for the CBT windings, and the $\mathcal{R}_{AD}$ and the $\mathcal{R}_{BC}$ can be calculated by

$$\begin{cases} \mathcal{R}_{AD} = \dfrac{(\mathcal{R}_{AA} + \mathcal{R}_{LA})(\mathcal{R}_{AD} + \mathcal{R}_{LD})}{\mathcal{R}_{AA} + \mathcal{R}_{LA} + \mathcal{R}_{AD} + \mathcal{R}_{LD}} \\ \mathcal{R}_{BC} = \dfrac{(\mathcal{R}_{AB} + \mathcal{R}_{LB})(\mathcal{R}_{AC} + \mathcal{R}_{LC})}{\mathcal{R}_{AB} + \mathcal{R}_{LB} + \mathcal{R}_{AC} + \mathcal{R}_{LC}} \end{cases} \tag{6}$$

In order to verify the proposed reluctance model, a customized magnetic core is built and experimentally tested, whose measurement results are given in Table II. It can be found that the calculated inductance from the reluctance model matches well with the measurement results and the 3D FEA simulation can be also adopted to estimate the inductance for the proposed structure. The ferrite material of the customized core is ML91S from HITACHI and all the inductance is measured by the impedance analyzer HP4292A.

IV. Experimental Validation and Discussion

In order to verify the proposed structure, two proof-of-concept prototypes are built and tested at 1 MHz switching frequency, whose key components list is given in Table III. Firstly, the prototype of two-phase synchronous buck converter with CI but without the integrated CBT is tested at 12V input and 4 V/6 A output, whose thermal image is shown in Fig. 7(a). The temperature rise of phase 2 on this prototype is higher that of phase 1 during the steady-state operation, due to the unbalanced current issue. The hot spot on the converter

TABLE I
CALCULATED RELUCTANCE OF THE PROPOSED STRUCTURE

Parameter	Description	Equation
$\mathcal{R}_{TW}/\mathcal{R}_{BW}$	Top/ Bottom plate for the CI	$\frac{w-a}{\mu_r\mu_0 tl}$
$\mathcal{R}_{TL}/\mathcal{R}_{BL}$	Top/ Bottom plate for the CBT	$\frac{l-b}{\mu_r\mu_0 tw}$
$\mathcal{R}_{AA}/\mathcal{R}_{AB}$	Air-gap for A, B	$\frac{g_1}{\mu_0 ab}$
$\mathcal{R}_{AC}/\mathcal{R}_{AD}$	Air-gap for C, D	$\frac{g_2}{\mu_0 ab}$
$\mathcal{R}_{LA}/\mathcal{R}_{LB}$	Leg A and B	$\frac{h-g_1}{\mu_r\mu_0 ab}$
$\mathcal{R}_{LC}/\mathcal{R}_{LD}$	Leg C and D	$\frac{h-g_2}{\mu_r\mu_0 ab}$

TABLE II
EXPERIMENTAL VERIFICATION OF THE PROPOSED RELUCTANCE MODEL

Geometry(mm)		Inductance (nH)			
w/l	11	1 turn	Calculation	Simulation	Measurement
a/b	4	L_{S1}/L_{S2}	187.14	175.64/ 173.32	184.34/ 186.45
h	4.5				
t	3	M	187.14	167.36	174.33
p	1.5				
g1	0.15	M_{CBT}	187.14	178.98	176.76
g2	0.15				

occurs at the phase 2 and its temperature reaches 83.9 °C during the steady-state operation. In addition, the drain-to-source and gate-to-source voltages of the high-side switches in this prototype are measured, whose waveforms are illustrated in Fig. 8 (a) and (b). It can be found that the while the switch Q3 achieves the ZVS turn-on in phase 2, the switch at the other phase Q1 lost the ZVS turn-on due to a higher current ripple. Thus, a reverse conduction occurs on this phase, which causes much power loss during the high-frequency operation.

As a comparison, the prototype with the proposed magnetic structure including the integrated CBT is also built and tested, whose thermal image is shown in Fig. 7(b) under the same specification. It can be found that the hot spot occurs on the gate drivers and the temperature of two phases maintains identical. Correspondingly, the drain-to-source and gate-to-source voltages of the high-side switches are illustrated in Fig. 8 (c) and (d). It can be found that with the integrated CBT, both of the high-side switches achieve the ZVS turn-on, which verifies the concept to solve the current unbalance issue by the proposed magnetic structure. In Fig. 9 (a), the tested efficiency of the prototype at different input voltages is presented. The prototype with integrated CBT can achieve the efficiency of 97.5% at 12V input and 4 V/ 6 A output while on the prototype without the integrated CBT, the efficiency drops as 94.9% due to extra power loss produced by the GaN FET with reverse conduction. The loss breakdown at the 24 W output and 97.5% efficiency is given in Fig. 9 (b). From the loss breakdown it is known that the power loss on the magnetic device contributes 35% of the total loss and the loss on the switch contributes 44% of the total power loss.

TABLE III
KEY PARAMETERS OF THE PROOF-OF-CONCEPT PROTOTYPE

Component	Value	Description
Switches (Q1-Q4)	EPC2015C	40V GaN HEMT
Gate drivers	LMG1205	Half-bridge gate driver
Core	EI-11-7.5	Customized core
C_{in}	25 V/ 2.2 uF × 8	Input capacitors
C_o	10 V/ 1 uF ×5	Output capacitors

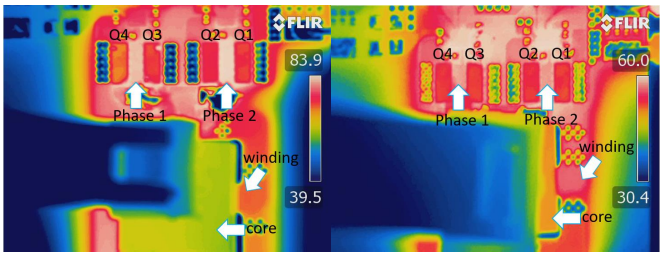

(a) (b)

Fig. 7. Thermal image of prototypes at 12 V input and 4 V/ 6 A output (a) without the integrated CBT (b) with the integrated CBT.

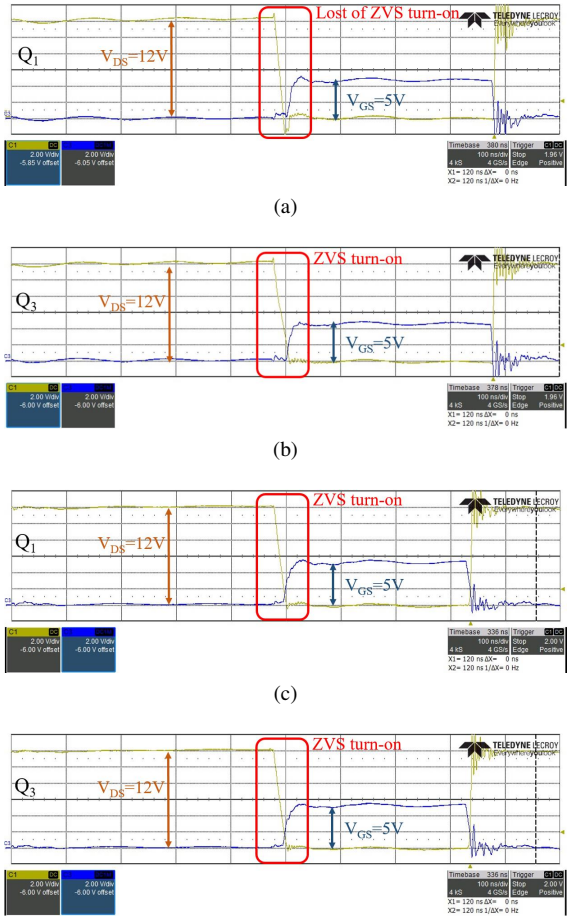

Fig. 8. Waveform of drain-to-source and gate-to-source voltage of high-side switches on the prototypes (a) Q1 without integrated CBT (b) Q3 without integrated CBT (c) Q1 with integrated CBT (d) Q3 with integrated CBT.

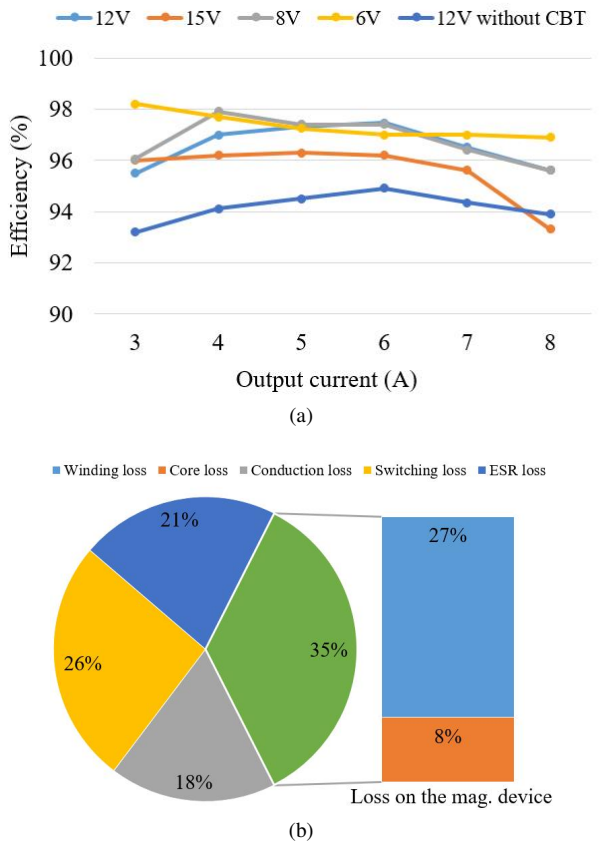

Fig. 9. Experimental efficiency of the prototype (a) Tested efficiency of the 1 MHz prototypes with different input voltage (b) Power loss breakdown at 12 V input and 4 V/ 6 A output.

V. Conclusion

This letter proposed an integrated magnetic structure of the coupled inductor and the current balancing transformer for high-frequency DC-DC converters. With multi-phase synchronous operation, the high current can be distributed directly into several phases with reduced power loss and simplified control method. The magnetic reluctance model is built for the proposed structure to guide the design for other applications. The proof-of-concept prototypes are built to verify the applicable capability for the structure and a high efficiency of 97.5% is achieved by the prototype at 1 MHz operation and 6 A output.

References

[1] X. Huang, Q. Li, Z. Liu, and F. C. Lee, "Analytical loss model of high voltage gan hemt in cascode configuration," *IEEE Transactions on Power Electronics*, vol. 29, no. 5, pp. 2208–2219, 2014.

[2] X. Huang, F. C. Lee, Q. Li, and W. Du, "High-frequency high-efficiency gan-based interleaved crm bidirectional buck/boost converter with inverse coupled inductor," *IEEE Transactions on Power Electronics*, vol. 31, no. 6, pp. 4343–4352, 2016.

[3] Z. Liu, F. C. Lee, Q. Li, and Y. Yang, "Design of gan-based mhz totem-pole pfc rectifier," *IEEE Journal of Emerging and Selected Topics in Power Electronics*, vol. 4, no. 3, pp. 799–807, 2016.

[4] X. Huang, F. C. Lee, Q. Li, and W. Du, "High-frequency high-efficiency gan-based interleaved crm bidirectional buck/boost converter with inverse coupled inductor," *IEEE Transactions on Power Electronics*, vol. 31, no. 6, pp. 4343–4352, 2016.

[5] Z. Liu, Z. Huang, F. C. Lee, and Q. Li, "Digital-based interleaving control for gan-based mhz crm totem-pole pfc," *IEEE Journal of Emerging and Selected Topics in Power Electronics*, vol. 4, no. 3, pp. 808–814, Sep. 2016.

[6] N. Lecic, G. Stojanovic, S. Djuric, and E. Laboure, "Design and analysis of planar symmetric six-phase coupled inductors," *IEEE Transactions on Magnetics*, vol. 51, no. 6, pp. 1–8, June 2015.

[7] F. Yang, X. Ruan, Y. Yang, and Z. Ye, "Interleaved critical current mode boost pfc converter with coupled inductor," *IEEE Transactions on Power Electronics*, vol. 26, no. 9, pp. 2404–2413, Sep. 2011.

[8] Q. Huang, R. Yu, Q. Ma, and A. Q. Huang, "Predictive zvs control with improved zvs time margin and limited variable frequency range for a 99efficient, 130-w/in3 mhz gan totem-pole pfc rectifier," *IEEE Transactions on Power Electronics*, vol. 34, no. 7, pp. 7079–7091, July 2019.

[9] Z. Ouyang, Y. Dou, and M. A. E. Andersen, "Integrated coupled inductors and current balancing transformer patent," 2019, patent P5137EP00 (pending).

[10] Z. Ouyang, G. Sen, O. C. Thomsen, and M. A. E. Andersen, "Analysis and design of fully integrated planar magnetics for primary–parallel isolated boost converter," *IEEE Transactions on Industrial Electronics*, vol. 60, no. 2, pp. 494–508, Feb 2013.